

Band-Geometric Origin of Superconducting Diode Effect

Jin-Xin Hu,¹ Shuai A. Chen,² and K. T. Law²

¹*Division of Physics and Applied Physics, School of Physical and Mathematical Sciences, Nanyang Technological University, Singapore 637371*

²*Department of Physics, Hong Kong University of Science and Technology, Clear Water Bay, Hong Kong, China*

The nonreciprocal critical supercurrents endow the superconducting diode effect (SDE) in noncentrosymmetric superconductors with time-reversal symmetry breaking. Recently, it was reported that the SDE has been observed in narrow-band superconductors such as twisted trilayer graphene with zero magnetic field. In this work, we unveil the SDE in superconductors that host narrow bands near Fermi energy, where the supercurrent has a significant contribution from the wave-function quantum geometry. By establishing the phenomenological Ginzburg-Landau theory, we show that besides the conventional band dispersion effect arising from the Fermi surface asymmetry, the microscopic origin of SDE from quantum geometry is the *quantum metric dipole*. Importantly, in the flat-band limit where the attractive interaction strength is much larger than the bandwidth, the supercurrent and diode effect contributed from quantum geometry becomes the leading order. The interaction-driven valley polarization which lifts the valley degeneracy is also necessary. Our work reveals a band-geometric origin of nonreciprocity in narrow-band superconductors.

Introduction.—The nonreciprocal response has attracted considerable interest due to its fundamental role in quantum materials and devices [1, 2]. Specifically, in the context of superconductors, researchers have observed a nonreciprocal phenomenon known as the superconducting diode effect (SDE) [3–5] in the bulk superconductors [6–10] and the Josephson junctions [11–14]. SDE is distinguished by the asymmetric behavior of critical or depairing supercurrents between the right and left directions. It is believed that the breaking of inversion (\mathcal{P}) and time-reversal (\mathcal{T}) symmetries is essential for the SDE to manifest. In understanding the SDE, many theoretical mechanisms have been proposed [15–29], and these explorations primarily focus on the deformation of Fermi surface, that is, the change of the band dispersions, such as Zeeman effect [16–18] or trigonal warping [22, 27].

Nevertheless, the role of the quantum geometric effect of wave functions, as an exclusively multi-band effect, remains relatively unexplored in shaping the SDE, particularly in the context of flat-band superconductors. In a flat-band superconductor for which the conventional BCS relation fails since the Fermi velocity vanishes, the wave-function quantum geometry can define the superfluidity and the coherence length [30–38]. Thus the quantum geometric effect can be considered as an additional degree of freedom to manipulate the physical properties apart from the electronic band structures. Therefore, investigating the interplay between the quantum geometric effect and the SDE is of fundamental importance which also holds the potential for driving further experimental developments.

The discovery of moiré superconductors such as magic angle twisted bilayer graphene provides a platform for exploring the flat-band superconductivity, and sizable supercurrents were observed in these experiments [39–43]. The non-dissipative transport in the moiré superconductors is associated with the finite superfluid weight, primarily governed by quantum geometry [34, 44–46]. On the other hand, the observation of the SDE in twisted tri-

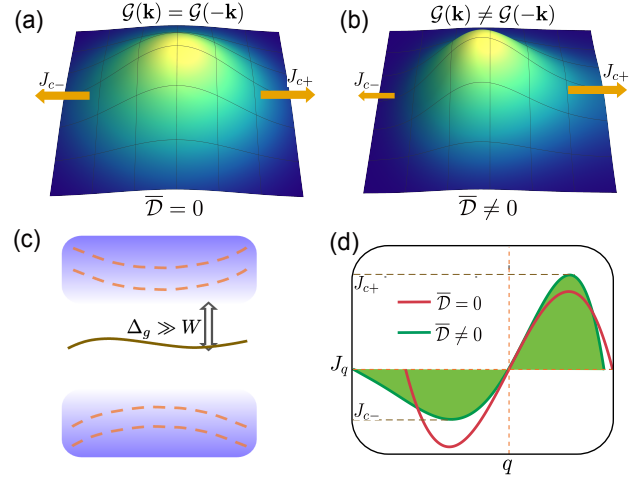


FIG. 1. (a) The profile of quantum metric \mathcal{G} in the momentum space. The depairing current is reciprocal with $|J_{c+}| = |J_{c-}|$. In this case, the preservation of \mathcal{P} enforces that the $\mathcal{G}(\mathbf{k})$ satisfies $\mathcal{G}(\mathbf{k}) = \mathcal{G}(-\mathbf{k})$, and the average of the quantum metric dipole $\bar{\mathcal{D}}$ is 0. (b) In the case of $\mathcal{G}(\mathbf{k}) \neq \mathcal{G}(-\mathbf{k})$, the presence of a non-zero $\bar{\mathcal{D}}$ results in $|J_{c+}| \neq |J_{c-}|$. The \mathcal{T} symmetry is already broken by valley polarization. (c) A multi-band system with an isolated flat band at the Fermi energy, and the band gap Δ_g separating it from other bands (depicted by the orange dashed lines) is significantly larger than the bandwidth W . (d) A schematic illustration of the current- q relation for (a) and (b), where q is the Cooper pair momentum.

layer graphene (tTLG) with vanishing spin-orbital coupling is particularly interesting [8]. This phenomenon is notable for its manifestation in the absence of a magnetic field and the presence of narrow bands near the Fermi energy.

Motivated by the recent experimental progresses, one fundamental question arises: Can quantum geometry play any role in the nonreciprocal SDE? In this work, we unveil the SDE originating from quantum geometry

of the Bloch wavefunction. Explicitly, we consider an isolated narrow band with the energy $\epsilon_{\mathbf{k}}$ while the wavefunction $|u_{\mathbf{k}}\rangle$ possesses finite quantum metric \mathcal{G} defined as

$$\mathcal{G}_{ab}(\mathbf{k}) = \text{Re}[\langle \partial_a u_{\mathbf{k}} | \partial_b u_{\mathbf{k}} \rangle - \langle \partial_a u_{\mathbf{k}} | u_{\mathbf{k}} \rangle \langle u_{\mathbf{k}} | \partial_b u_{\mathbf{k}} \rangle], \quad (1)$$

where $\partial_a = \partial/\partial k_a$ is the momentum derivative. By establishing the Ginzburg-Landau theory around the transition region, we study the dissipationless supercurrent as well as the feasibility of SDE (see Fig. 1). Importantly, the geometric origin of SDE is the distribution of quantum metric dipole with the expression as

$$\mathcal{D}_a^{bc}(\mathbf{k}) = \partial_a \mathcal{G}_{bc}(\mathbf{k}). \quad (2)$$

The average of quantum metric dipole $\overline{\mathcal{D}_a^{bc}}$ [see Eq. (11)] over the first Brillouin zone can be finite when the \mathcal{P} symmetry is broken [see Fig.1 (a), (b)]. The SDE can show up when the \mathcal{T} symmetry is also violated. By utilizing the phenomenological analysis, we calculate the Ginzburg-Landau coefficients for a Haldane-like model with flattened bands which consists of finite quantum metric and a non-zero quantum metric dipole. Furthermore, we discuss the potential application of this theoretical framework to moiré superconductors, specifically twisted trilayer graphene (tTLG), which exhibits narrow bands near the Fermi energy. The implications of our findings can provide valuable insights for experimental investigations in this field.

Ginzburg-Landau theory for SDE.—To elucidate the fundamental physical properties, we consider a multi-band system which possesses an isolated flat band near Fermi energy as shown in Fig. 1 (c). There a large band gap Δ_g significantly exceeding the bandwidth of the isolated band W . Initially, we have $H = H_0 + H_{\text{int}}$, where the non-interacting H_0 describes the band structure of bare electron $a_{\sigma}(\mathbf{r})$. For simplicity, we focus on s -wave pairing and H_{int} involves the effective attractive interaction

$$H_{\text{int}} = -U \int d\mathbf{r} a_{+}^{\dagger}(\mathbf{r}) a_{-}^{\dagger}(\mathbf{r}) a_{-}(\mathbf{r}) a_{+}(\mathbf{r}), \quad (3)$$

where U denotes attractive interaction strength, and $\sigma = \pm$ denotes the valley index. Owing to the large band gap, we make the projection onto the isolated band, $a_{\sigma}(\mathbf{r}) \rightarrow \sum_{\alpha\mathbf{k}} u_{\alpha\sigma}^*(\mathbf{k}) c_{\mathbf{k}\sigma} e^{i\mathbf{k}\cdot\mathbf{r}}$ with α being the orbital degrees of freedom. Here the operator $c_{\mathbf{k}\sigma}$ annihilates a fermion on the isolated band with Bloch wave function $u_{\alpha\sigma}(\mathbf{k})$. Meanwhile, the free part H_0 is mapped to $H_0 = \sum_{\mathbf{k}\sigma} \epsilon_{\mathbf{k}\sigma} c_{\mathbf{k}\sigma}^{\dagger} c_{\mathbf{k}\sigma}$ with $\epsilon_{\mathbf{k}\sigma}$ being the dispersion spectrum. To deal with the attractive interaction, we introduce the auxiliary Cooper pair operator $\Delta(\mathbf{r}) = -U a_{-}(\mathbf{r}) a_{+}(\mathbf{r})$, which gives rise to $H_{\text{int}} = \int d\mathbf{r} \Delta(\mathbf{r}) a_{+}^{\dagger}(\mathbf{r}) a_{-}^{\dagger}(\mathbf{r}) + h.c.$. After the Fourier transformation and the band projection, we have

$$H_{\text{int}} = \sum_{\mathbf{k}, \mathbf{q}} \Gamma(\mathbf{k}, \mathbf{q}) \Delta_{\mathbf{q}} c_{\mathbf{k}+\mathbf{q},+}^{\dagger} c_{-\mathbf{k},-}^{\dagger} + h.c.. \quad (4)$$

Here the form factor $\Gamma(\mathbf{k}, \mathbf{q}) = \langle u_{\mathbf{k}+\mathbf{q},+} | u_{-\mathbf{k},-}^* \rangle$ as the overlap between Bloch waves, encodes the quantum metric of the Bloch waves which was demonstrated to play a key role in a flat-band superconductors [30, 37, 38].

In general, one may have $u_{\mathbf{k},+} \neq u_{-\mathbf{k},-}^*$ due to the absence of the \mathcal{T} symmetry. Throughout this work, we focus on the case where the breaking of the \mathcal{T} symmetry is manifested by the polarization effect of two flavors σ . For example in the model in Eq. (3), we assume a valley polarized order δ_v by changing $\epsilon_{\mathbf{k}\sigma}$ to $\epsilon_{\mathbf{k}\sigma} + \sigma\delta_v$, which preserves the $U_v(1)$ symmetry [8, 27, 47–50]. Thus the wavefunctions maintain as $u_{\mathbf{k},+} = u_{-\mathbf{k},-}^*$. The form factor $\Gamma(\mathbf{k}, \mathbf{q})$ can be expanded as $|\Gamma(\mathbf{k}, \mathbf{q})|^2 = 1 - \sum_{ab} \mathcal{G}_{ab}(\mathbf{k}) q_a q_b + \mathcal{O}(q^3)$ with \mathcal{G}_{ab} being the quantum metric in Eq. (1). Around the transition region, one may derive the grand potential $F = \int_{\mathbf{q}} \mathcal{F}[\Delta_{\mathbf{q}}]$ with the free energy density up to the fourth order of $|\Delta_{\mathbf{q}}|^4$, yielding

$$\mathcal{F}[\Delta_{\mathbf{q}}] = (a_0 + a_{\mathbf{q}}) |\Delta_{\mathbf{q}}|^2 + \frac{b}{2} |\Delta_{\mathbf{q}}|^4. \quad (5)$$

The coefficients a_0 and b are momentum-independent,

$$a_0 = \frac{1}{W} \tanh \frac{\beta_c W \bar{T}}{4}, \quad (6)$$

$$b = \frac{\beta_c}{2W^3} \left(W - \frac{4}{\beta_c} \tanh \frac{\beta_c W}{4} \right), \quad (7)$$

where $\bar{T} = (T - T_c)/T_c$ is the dimensionless temperature parameter and $T_c = \beta_c^{-1}$ denotes the mean-field transition temperature. In particular, $T_c \approx U/4$ for a narrow band $W \ll U$. The $a_{\mathbf{q}}$ describes the dynamics of the Cooper pair $\Delta_{\mathbf{q}}$, and originates from both the conventional band dispersion and the quantum geometry $a_{\mathbf{q}} = a_{\mathbf{q}}^c + a_{\mathbf{q}}^g$. The quantum metric contribution vanishes identically in a single-band system, which indicates that $a_{\mathbf{q}}^g$ represents the intrinsic multi-band effect. Due to the absence of \mathcal{T} symmetry, we can have terms with odd orders of \mathbf{q} which will account for the SDE. To proceed, we consider a system that respects a C_3 symmetry and tTLG belongs to this case. By parametrizing $\mathbf{q} = q(\cos\theta, \sin\theta)$ with θ being the angle between \mathbf{q} and the principle axis, we have the following expression up to the q^3 ,

$$a_{\mathbf{q}}^c = \frac{\beta_c}{4} [\lambda_c q^2 + \delta_v \alpha(\theta) q^3]. \quad (8)$$

$$a_{\mathbf{q}}^g = \frac{\beta_c}{4} [\overline{\mathcal{G}} q^2 + \delta_v \overline{\mathcal{D}}(\theta) q^3], \quad (9)$$

where we consider δ_v as a perturbation $\delta_v \ll W$ and the C_3 symmetry ensures that $\overline{\mathcal{G}}_{xx} = \overline{\mathcal{G}}_{yy} \equiv \overline{\mathcal{G}}$ and $\overline{\mathcal{G}}_{xy} = \overline{\mathcal{G}}_{yx} = 0$. One may immediately obtain a relation for the effective mass [37, 38] of Cooper pairs $\frac{1}{2m^*} = \beta_c [\lambda_c + \overline{\mathcal{G}}]/4$ with the averaged $\overline{\mathcal{G}}_{ab}$ over the first Brillouin zone, yielding

$$\overline{\mathcal{G}}_{ab} = \sum_{\mathbf{k}} \mathcal{G}_{ab}(\mathbf{k}) w_{\mathbf{k}}, \quad (10)$$

with the weight $w_{\mathbf{k}} = \tanh(\beta_c \varepsilon_{\mathbf{k}}/2)/(\beta_c \varepsilon_{\mathbf{k}}/2)$ and $\varepsilon_{\mathbf{k}} = \epsilon_{\mathbf{k}+} - \mu$. In Eqs. (8) and (9), the coefficients before q^3 depend on the angle θ , $\alpha(\theta) = \alpha_x^{xx} \cos 3\theta - \alpha_y^{yy} \sin 3\theta$ and $\bar{\mathcal{D}}(\theta) = \bar{\mathcal{D}}_x^{xx} \cos 3\theta - \bar{\mathcal{D}}_y^{yy} \sin 3\theta$. Here α_a^{bc} is a tensor for Fermi surface asymmetry and $\bar{\mathcal{D}}_a^{bc}$ is the weighted averaged quantum metric dipole with

$$\bar{\mathcal{D}}_a^{bc} = -\beta_c \sum_{\mathbf{k}} \partial_a [\mathcal{G}_{bc}(\mathbf{k}) w_{\mathbf{k}}] f_{\varepsilon_{\mathbf{k}}}, \quad (11)$$

with the Fermi-Dirac distribution $f_{\varepsilon_{\mathbf{k}}} = 1/(1+e^{\beta_c \varepsilon_{\mathbf{k}}})$. By breaking inversion \mathcal{P} symmetry, $\mathcal{G}(\mathbf{k}) \neq \mathcal{G}(-\mathbf{k})$ leads to $\bar{\mathcal{D}}_a^{bc} \neq 0$ as illustrated in Figs. 1 (a) and (b). In the flat-band limit of $W \ll U$, we have $a_0 \rightarrow \bar{T}/4T_c$, $b \rightarrow \beta_c^3/96$, $\bar{\mathcal{G}} \rightarrow \sum_{\mathbf{k}} \mathcal{G}_{ab}(\mathbf{k})$ and $\bar{\mathcal{D}}_a^{bc} \rightarrow \beta_c^2/4 \sum_{\mathbf{k}} \mathcal{D}_a^{bc}(\mathbf{k}) \varepsilon_{\mathbf{k}}$, which is related to Eq. (2). Besides the geometric terms, the conventional terms in a_q^c can be obtained as

$$\lambda_c = \frac{2}{\beta_c^2} \sum_{\mathbf{k}, n} v_x^2 G_e^2 G_h^2, \quad (12)$$

and

$$\alpha_a^{bc} = -\frac{4}{\beta_c^2} \sum_{\mathbf{k}, n} \left[\frac{1}{6} v_{abc} (2G_e^3 G_h - G_e^2 G_h^2) + v_{ab} v_c \right. \\ \left. (3G_e^4 G_h - G_e^3 G_h^2) + v_a v_b v_c (4G_e^5 G_h - G_e^4 G_h^2) \right], \quad (13)$$

where $v_a = \partial_a \varepsilon_{\mathbf{k}}$, $v_{ab} = \partial_{ab} \varepsilon_{\mathbf{k}}$ and $v_{abc} = \partial_{abc} \varepsilon_{\mathbf{k}}$. The Green's functions $G_e = (i\omega_n - \varepsilon_{\mathbf{k}})^{-1}$ and $G_h = (-i\omega_n - \varepsilon_{\mathbf{k}})^{-1}$ with $\omega_n = (2n+1)\pi/\beta_c$ being fermionic Matsubara frequencies. The details of the concrete model and derivations are in Supplementary Material (SM) II [51].

Phenomenologically, the supercurrent $J_{\mathbf{q}}$ can be derived as $J_{\mathbf{q}} = 2\partial \mathcal{F}_{\mathbf{q}}/\partial \mathbf{q}$, which gives $J_{\mathbf{q}} = -2/b(a_0 + a_{\mathbf{q}})\partial_{\mathbf{q}} a_{\mathbf{q}}$. $|\Delta_{\mathbf{q}}|$ has been obtained by minimizing $\mathcal{F}_{\mathbf{q}}$ as $\partial \mathcal{F}_{\mathbf{q}}/\partial |\Delta_{\mathbf{q}}| = 0$. With δ_v as a perturbation ($\delta_v \ll W$), the critical current occurs at the momentum $q_c \approx \pm(-4a_0/[3\beta_c(\bar{\mathcal{G}} + \lambda_c)])^{1/2}$. As a result, we obtain the diode qualify factor $\eta = (J_{c+} - |J_{c-}|)/(J_{c+} + |J_{c-}|)$ as

$$\eta = \frac{\sqrt{3}}{3} |\bar{T}|^{1/2} (\bar{\mathcal{G}} + \lambda_c)^{-\frac{3}{2}} [\bar{\mathcal{D}}(\theta) + \alpha(\theta)] \delta_v. \quad (14)$$

The expression for η scales as $\sqrt{T_c - \bar{T}}$ in the vicinity of the transition temperature. Eq. (14) encapsulates the primary finding of our study. It is evident from Eq. (14) that, in addition to the conventional terms λ_c and α , the expression for η incorporates the quantum metric $\bar{\mathcal{G}}$ and the quantum metric dipole $\bar{\mathcal{D}}$. This insight underscores the significance of quantum geometric factors in determining SDE.

In the flat-band limit, where $U \gg W$, it follows that $\alpha_a^{bc} = \beta_c^2/24 \sum_{\mathbf{k}} v_{abc} + \mathcal{O}(\beta_c^4)$ and $\lambda_c = \beta_c^2/24 \sum_{\mathbf{k}} v_x^2 + \mathcal{O}(\beta_c^4)$, which vanishes at the order of $\mathcal{O}(\beta_c^4)$ and $\mathcal{O}(\beta_c^2)$, respectively [51]. This results in $\alpha/\bar{\mathcal{D}} \sim W^2/U^2$ and $a_q^c/a_q^g \sim W^2/U^2$, indicating that the supercurrent predominantly arises from quantum geometry. As a result,

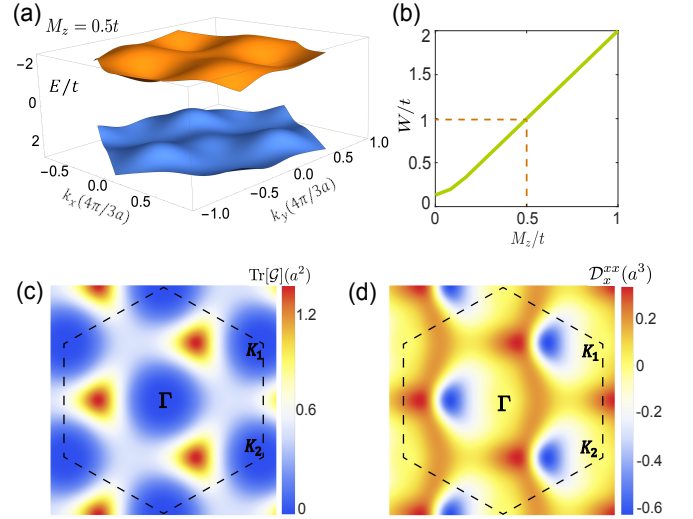


FIG. 2. (a) The band structure of the flattened Haldane model with the staggered potential term $M_z = 0.5t$. The bandwidth of the lower valence band is approximately $W \approx t$. (b) The bandwidth W as a function of M_z . (c), (d) Momentum-space quantum metric $\text{Tr}[\mathcal{G}]$ and quantum metric dipole \mathcal{D}_x^{xx} of the lower band within the first Brillouin zone, which are evaluated from Eq. (1) and (2). In the calculation, we take $t_A^+ = t_2 e^{i\pi/2}$, $t_B^+ = t_2 e^{-i\pi/2}$, $t_2 = 0.39t$ and $t_3 = -0.34t$. Here we denote t as the energy unit.

the quantum geometric contribution also dominates the diode effect in this limit. Fig. 1(d) provides a schematic depiction of the nonreciprocal current- q relation in the presence of $\bar{\mathcal{D}}$. Conversely, when the isolated band becomes highly dispersive, as $\beta_c W \gg 1$, the system transitions back to a conventional BCS regime. In this regime, quantum geometry plays a less significant role, as the averages of \mathcal{G} and \mathcal{D} involve weighted averages near the Fermi surface, which contribute minimally in the conventional scenario, as indicated in Eqs.(10) and (11) [51].

Several key points can be extracted from the Ginzburg-Landau framework: (i) The nonreciprocity of the supercurrent arises from its part Fermi surface asymmetry α and part quantum metric dipole $\bar{\mathcal{D}}$. (ii) Although the conventional and geometric supercurrents coexist in general cases, in the flat-band limit when $U \gg W$, the geometric part dominates over the conventional one. (iii) It is crucial to highlight that in the exact flat-band limit with $W = 0$, $\lambda_c = \alpha = \bar{\mathcal{D}} = 0$, and only $\bar{\mathcal{G}}$ is nonzero, leading to purely geometric supercurrent but no diode effect. In the following section, we will demonstrate these behaviors by calculating the Ginzburg-Landau coefficients for a Haldane-like flat-band model. Also for the realistic material such as moiré graphene, the main physics of the low-energy flat bands can be captured by a Haldane-like model [52].

Flat-band model study.—To illustrate the features of the Ginzburg-Landau theory for SDE developed above, we examine a Haldane-like model with two valleys and two orbitals (A and B) per-site on the triangular lattice

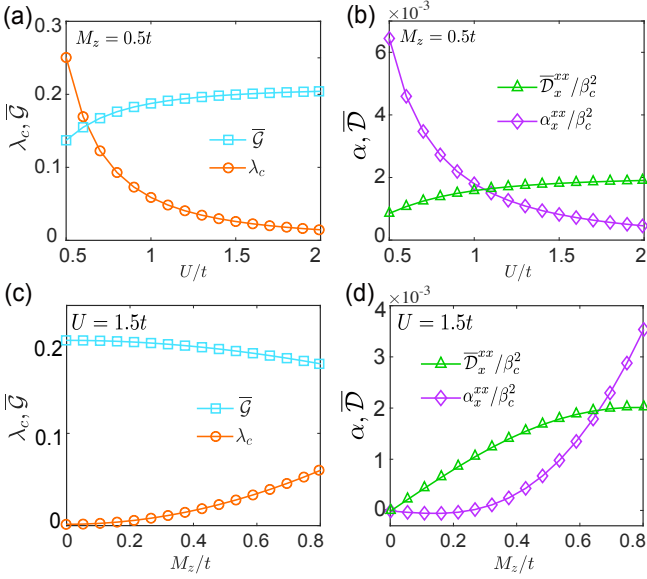


FIG. 3. The calculations of the Ginzburg-Landau coefficients for (a) λ_c , $\bar{\mathcal{G}}$ and (b) α_x^{xx} , $\bar{\mathcal{D}}_x^{xx}$ as a function of the attractive interaction U at $M_z = 0.5t$. At large U , $\bar{\mathcal{G}} \gg \lambda_c$ and $\bar{\mathcal{D}}_x^{xx} \gg \alpha_x^{xx}$. (c) λ_c , $\bar{\mathcal{G}}$ and (d) α_x^{xx} , $\bar{\mathcal{D}}_x^{xx}$ as a function of M_z at $U = 1.5t$. The Fermi energy is at $\mu = -2t$.

[3], which has the form in real space

$$\begin{aligned}
 h_0^\sigma = & - \sum_{\langle ij \rangle} t a_{i\sigma}^\dagger b_{j\sigma} - \sum_{\langle ij \rangle'} t_A^\sigma a_{i\sigma}^\dagger a_{j\sigma} + t_B^\sigma b_{i\sigma}^\dagger b_{j\sigma} \\
 & - \sum_{\langle ij \rangle''} t_3 a_{i\sigma}^\dagger b_{j\sigma} + \sum_i M_z (a_{i\sigma}^\dagger a_{i\sigma} - b_{i\sigma}^\dagger b_{i\sigma}), \quad (15)
 \end{aligned}$$

where $\langle ij \rangle$, $\langle ij \rangle'$ and $\langle ij \rangle''$ represent the first, second and third nearest neighbor hoppings, respectively. $\sigma = \pm 1$ denotes the valley, and operator $a(b)_{i\sigma}$ annihilates a fermion with σ valley in the orbital $A(B)$ on site i . M_z is the staggered potential term on the A and B orbitals. Due to \mathcal{T} symmetry, $t_X^- = (t_X^+)^*$. The energy spectrum of the model is shown in Fig. 2(a), which exhibits a pair of narrow bands at $E \approx \pm 2t$. It is straightforward to obtain the momentum-space distribution of the quantum metric and quantum metric dipole for the lower band from Eq. (1) and (2) as plotted in Fig. 2(c) and (d). In Fig. 2(b), increasing M_z enhances the bandwidth W . Evidently, M_z breaks \mathcal{P} symmetry, leading to $\mathcal{G}_{ab}(\mathbf{k}) \neq \mathcal{G}_{ab}(-\mathbf{k})$.

We calculate the Ginzburg-Landau coefficients from Eq. (10) to Eq. (13), where the Fermi energy resides on the lower band, as depicted in Fig. 2(a). Fig. 3(a) displays the quadratic terms λ_c and $\bar{\mathcal{G}}$, plotted as functions of U . As expected, $\bar{\mathcal{G}}$ reaches its optimal value at high values of U , while λ_c exhibits a power-law decay, scaling as $1/U^2$. Consequently, the supercurrent contribution from the quantum metric becomes predominant over the conventional component in the regime of large U . In Fig. 3(b), we illustrate the cubic terms α_x^{xx} and $\bar{\mathcal{D}}_x^{xx}$, which decay as $1/U^2$ and $1/U^4$, respectively. Clearly, the

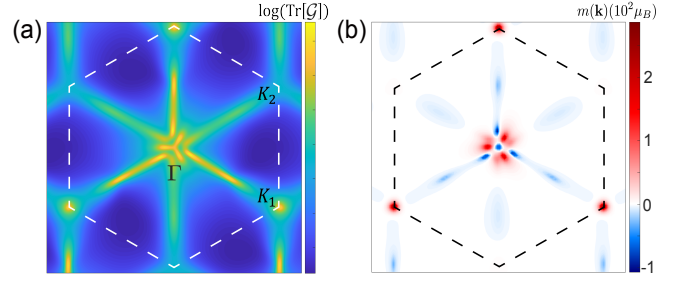


FIG. 4. Momentum-space profile of (a) the quantum metric $\text{Tr}[\mathcal{G}]$ and (b) the orbital magnetic moment $m(\mathbf{k})$ of the lowest conduction band in tTLG.

nonreciprocal term, driven by the quantum metric dipole, overshadows the conventional Fermi surface asymmetry term α_x^{xx} . Furthermore, the staggered potential term M_z , which violates \mathcal{P} symmetry, plays a critical role in the SDE. This is shown Fig. 3(c) and (d), where an increase in M_z causes λ_c to rise from nearly zero due to bandwidth enhancement, while $\bar{\mathcal{G}}$ remains almost unaffected. Fig. 3(d) shows that both $\bar{\mathcal{D}}_x^{xx}$ and α_x^{xx} vanish exactly when $M_z = 0$, yet display different trends as M_z increases. This behavior aligns with the understanding of Eq. (13), where α scales as W^3 at large W .

Related to moiré superconductors.—Experimentally, tTLG exhibits the SDE at the twist angle $\theta_t = 1.3^\circ$ and under a finite vertical displacement field. Through magnetic-field training, a nonzero interaction-driven valley polarization can be stabilized via valley-Zeeman coupling. The energy undergoes a change, given by $\epsilon_{\mathbf{k}\sigma} \rightarrow \epsilon_{\mathbf{k}\sigma} - \sigma m(\sigma \mathbf{k}) B_z$, where $m(\mathbf{k})$ is the orbital magnetic moment. Consequently, the valley polarization is approximated as $\delta_v \approx \sum_{\mathbf{k}} m(\mathbf{k}) B_z$. The momentum-profile of $m(\mathbf{k})$ is illustrated in Fig. 4 (b). The breaking of intra-valley \mathcal{P} symmetry ensures $\mathcal{G}_{ab}(\mathbf{k}) \neq \mathcal{G}_{ab}(-\mathbf{k})$, as depicted in Fig. 4 (a). Although the tTLG is a complicated multi-band system, we believe that the flat-band model we studied in the previous section can capture the main features of tTLG. We also provide more details of the Ginzburg-Landau coefficients for SDE in tTLG in SM IV [51].

Discussion.—In summary, we have formulated the Ginzburg-Landau theory for the SDE in narrow-band superconductors, with particular applicability to moiré graphene systems. Our work highlights the essential contributions of the quantum metric and quantum metric dipole to the non-dissipative transport and resulting in SDE. Interestingly, the quantum metric dipole plays a vital role in other nonreciprocal phenomena [54–56]. Although our phenomenological theory primarily focuses on C_3 symmetric systems with a specific way for breaking \mathcal{T} , it is highly general and the method can be extended to other cases as well. Additionally, since the Ginzburg-Landau analysis provides a phenomenological perspective near T_c and within the long-wavelength regime, we also support our theoretical framework through a mean-

field study of the supercurrent, providing a demonstration of the key principles underpinning our phenomenological theory [51].

Acknowledgements.—We appreciate inspiring discussions with Jiang-Xiazi Lin, Bo Yang and Justin C.

W. Song. K. T. L. acknowledges the support of the Ministry of Science and Technology, China, and Hong Kong Research Grant Council through Grants No. 2020YFA0309600, No. RFS2021-6S03, No. C6025-19G, No. AoE/P-701/20, No. 16310520, No. 16310219, No. 16307622, and No. 16309718.

-
- [1] Y. Tokura and N. Nagaosa, *Nature communications* **9**, 3740 (2018).
- [2] N. Nagaosa and Y. Yanase, *Annual Review of Condensed Matter Physics* **15** (2023).
- [3] R. Wakatsuki and N. Nagaosa, *Physical Review Letters* **121**, 026601 (2018).
- [4] K. Jiang and J. Hu, *Nature Physics* **18**, 1145 (2022).
- [5] M. Nadeem, M. S. Fuhrer, and X. Wang, *Nature Reviews Physics*, 1 (2023).
- [6] F. Ando, Y. Miyasaka, T. Li, J. Ishizuka, T. Arakawa, Y. Shiota, T. Moriyama, Y. Yanase, and T. Ono, *Nature* **584**, 373 (2020).
- [7] Y.-Y. Lyu, J. Jiang, Y.-L. Wang, Z.-L. Xiao, S. Dong, Q.-H. Chen, M. V. Milošević, H. Wang, R. Divan, J. E. Pearson, *et al.*, *Nature communications* **12**, 2703 (2021).
- [8] J.-X. Lin, P. Siriviboon, H. D. Scammell, S. Liu, D. Rhodes, K. Watanabe, T. Taniguchi, J. Hone, M. S. Scheurer, and J. Li, *Nature Physics* **18**, 1221 (2022).
- [9] H. Narita, J. Ishizuka, R. Kawarazaki, D. Kan, Y. Shiota, T. Moriyama, Y. Shimakawa, A. V. Ognev, A. S. Samardak, Y. Yanase, *et al.*, *Nature Nanotechnology* **17**, 823 (2022).
- [10] Y. Hou, F. Nichele, H. Chi, A. Lodesani, Y. Wu, M. F. Ritter, D. Z. Haxell, M. Davydova, S. Ilić, O. Glezakou-Elbert, *et al.*, *Physical Review Letters* **131**, 027001 (2023).
- [11] H. Wu, Y. Wang, Y. Xu, P. K. Sivakumar, C. Pasco, U. Filippozzi, S. S. Parkin, Y.-J. Zeng, T. McQueen, and M. N. Ali, *Nature* **604**, 653 (2022).
- [12] B. Pal, A. Chakraborty, P. K. Sivakumar, M. Davydova, A. K. Gopi, A. K. Pandeya, J. A. Krieger, Y. Zhang, M. Date, S. Ju, *et al.*, *Nature physics* **18**, 1228 (2022).
- [13] J. Díez-Mérida, A. Díez-Carlón, S. Yang, Y.-M. Xie, X.-J. Gao, J. Senior, K. Watanabe, T. Taniguchi, X. Lu, A. P. Higginbotham, *et al.*, *Nature Communications* **14**, 2396 (2023).
- [14] M. Trahms, L. Melischek, J. F. Steiner, B. Mahendru, I. Tamir, N. Bogdanoff, O. Peters, G. Reecht, C. B. Winkelmann, F. von Oppen, *et al.*, *Nature* **615**, 628 (2023).
- [15] B. Zinkl, K. Hamamoto, and M. Sigrist, *Physical Review Research* **4**, 033167 (2022).
- [16] N. F. Yuan and L. Fu, *Proceedings of the National Academy of Sciences* **119**, e2119548119 (2022).
- [17] J. J. He, Y. Tanaka, and N. Nagaosa, *New Journal of Physics* **24**, 053014 (2022).
- [18] A. Daido, Y. Ikeda, and Y. Yanase, *Physical Review Letters* **128**, 037001 (2022).
- [19] S. Ilić and F. S. Bergeret, *Physical Review Letters* **128**, 177001 (2022).
- [20] A. Daido and Y. Yanase, *Physical Review B* **106**, 205206 (2022).
- [21] B. Zhai, B. Li, Y. Wen, F. Wu, and J. He, *Physical Review B* **106**, L140505 (2022).
- [22] H. D. Scammell, J. Li, and M. S. Scheurer, *2D Materials* **9**, 025027 (2022).
- [23] H. F. Legg, D. Loss, and J. Klinovaja, *Physical Review B* **106**, 104501 (2022).
- [24] M. Davydova, S. Prembabu, and L. Fu, *Science advances* **8**, eabo0309 (2022).
- [25] Y. Zhang, Y. Gu, P. Li, J. Hu, and K. Jiang, *Physical Review X* **12**, 041013 (2022).
- [26] Y.-M. Xie and K. Law, *Physical Review Letters* **131**, 016001 (2023).
- [27] J.-X. Hu, Z.-T. Sun, Y.-M. Xie, and K. Law, *Physical Review Letters* **130**, 266003 (2023).
- [28] J. J. He, Y. Tanaka, and N. Nagaosa, *Nature Communications* **14**, 3330 (2023).
- [29] S. Banerjee and M. S. Scheurer, *Physical Review Letters* **132**, 046003 (2024).
- [30] S. Peotta and P. Törmä, *Nature communications* **6**, 8944 (2015).
- [31] A. Julku, S. Peotta, T. I. Vanhala, D.-H. Kim, and P. Törmä, *Physical review letters* **117**, 045303 (2016).
- [32] L. Liang, T. I. Vanhala, S. Peotta, T. Siro, A. Harju, and P. Törmä, *Physical Review B* **95**, 024515 (2017).
- [33] N. Verma, T. Hazra, and M. Randeria, *Proceedings of the National Academy of Sciences* **118**, e2106744118 (2021).
- [34] P. Törmä, S. Peotta, and B. A. Bernevig, *Nature Reviews Physics* **4**, 528 (2022).
- [35] J. Herzog-Arbeitman, V. Peri, F. Schindler, S. D. Huber, and B. A. Bernevig, *Physical review letters* **128**, 087002 (2022).
- [36] P. Törmä, *Physical Review Letters* **131**, 240001 (2023).
- [37] S. A. Chen and K. Law, *Physical Review Letters* **132**, 026002 (2024).
- [38] J.-X. Hu, S. A. Chen, and K. Law, *arXiv preprint arXiv:2308.05686* (2023).
- [39] Y. Cao, V. Fatemi, S. Fang, K. Watanabe, T. Taniguchi, E. Kaxiras, and P. Jarillo-Herrero, *Nature* **556**, 43 (2018).
- [40] M. Yankowitz, S. Chen, H. Polshyn, Y. Zhang, K. Watanabe, T. Taniguchi, D. Graf, A. F. Young, and C. R. Dean, *Science* **363**, 1059 (2019).
- [41] H. S. Arora, R. Polski, Y. Zhang, A. Thomson, Y. Choi, H. Kim, Z. Lin, I. Z. Wilson, X. Xu, J.-H. Chu, *et al.*, *Nature* **583**, 379 (2020).
- [42] M. Oh, K. P. Nuckolls, D. Wong, R. L. Lee, X. Liu, K. Watanabe, T. Taniguchi, and A. Yazdani, *Nature* **600**, 240 (2021).
- [43] H. Tian, X. Gao, Y. Zhang, S. Che, T. Xu, P. Cheung, K. Watanabe, T. Taniguchi, M. Randeria, F. Zhang, *et al.*, *Nature* **614**, 440 (2023).
- [44] X. Hu, T. Hyart, D. I. Pikulin, and E. Rossi, *Physical Review Letters* **123**, 237002 (2019).
- [45] A. Julku, T. J. Peltonen, L. Liang, T. T. Heikkilä, and P. Törmä, *Physical Review B* **101**, 060505 (2020).

- [46] F. Xie, Z. Song, B. Lian, and B. A. Bernevig, Physical review letters **124**, 167002 (2020).
- [47] H. C. Po, L. Zou, A. Vishwanath, and T. Senthil, Physical Review X **8**, 031089 (2018).
- [48] J. Y. Lee, E. Khalaf, S. Liu, X. Liu, Z. Hao, P. Kim, and A. Vishwanath, Nature communications **10**, 5333 (2019).
- [49] N. Bultinck, S. Chatterjee, and M. P. Zaletel, Physical review letters **124**, 166601 (2020).
- [50] Z. Han and S. A. Kivelson, Physical Review B **105**, L100509 (2022).
- [51] See Supplementary Material for: 1. BCS theory in the flat-band case; 2. Ginzburg-Landau theory for SDE; 3. Self-consistent mean-field study of supercurrent; 4. Application to moiré superconductors.
- [52] Y.-H. Zhang, D. Mao, and T. Senthil, Physical Review Research **1**, 033126 (2019).
- [3] S. Yang, Z.-C. Gu, K. Sun, and S. D. Sarma, Physical Review B **86**, 241112 (2012).
- [54] Y. Gao and D. Xiao, Physical review letters **122**, 227402 (2019).
- [55] A. Arora, M. S. Rudner, and J. C. Song, Nano Letters **22**, 9351 (2022).
- [56] D. Kaplan, T. Holder, and B. Yan, Physical Review Letters **132**, 026301 (2024).

Supplementary Material for “Quantum Geometric Origin of Superconducting Diode Effect”

Jin-Xin Hu,¹ Shuai A. Chen,² K. T. Law²

¹*Division of Physics and Applied Physics, School of Physical and Mathematical Sciences, Nanyang Technological University, Singapore 637371*

²*Department of Physics, Hong Kong University of Science and Technology, Clear Water Water Bay, Hong Kong, China*

I. BCS THEORY IN THE FLAT-BAND CASE

In this section we derive the BCS relations in the flat-band superconductors. We consider the system that a band is considered isolated when a substantial gap exists between the conduction and valence bands, allowing us to apply the projection technique. Additionally, we assume that there is only spin or valley degeneracy within the isolated band. By focusing on the isolated band, we can gain valuable insights into the behavior of the superconducting phase in multi-band systems. We assume the attractive interaction U on the flat band, and the total Hamiltonian can be written as

$$H = H_0 + H_{\text{int}} \quad (\text{S1})$$

where $H_0 = \sum_{\mathbf{k}, \sigma} \varepsilon_{\mathbf{k}} c_{\mathbf{k}\sigma}^\dagger c_{\mathbf{k}\sigma}$. The attractive interaction term accordingly is given by

$$H_{\text{int}} = -\frac{U}{N} \sum_{\mathbf{k}\mathbf{k}'} c_{\mathbf{k}\uparrow}^\dagger c_{-\mathbf{k}\downarrow}^\dagger c_{-\mathbf{k}'\downarrow} c_{\mathbf{k}'\uparrow}, \quad (\text{S2})$$

For a superconductor, we can introduce the s-wave order parameter on the band fermion,

$$\Delta = -\frac{U}{N} \sum_{\mathbf{k}} \langle c_{-\mathbf{k}\downarrow} c_{\mathbf{k}\uparrow} \rangle, \quad (\text{S3})$$

and by a proper gauge choice, we can set the order parameter Δ to be real-valued. Then one can derive a mean-field Hamiltonian

$$\begin{aligned} H_{\text{mf}} &= \sum_{\mathbf{k}} \left[(\varepsilon_{\mathbf{k}} - \mu) c_{\mathbf{k}\sigma}^\dagger c_{\mathbf{k}\sigma} + \Delta c_{\mathbf{k}\uparrow}^\dagger c_{-\mathbf{k}\downarrow}^\dagger + \Delta c_{-\mathbf{k}\downarrow} c_{\mathbf{k}\uparrow} \right] + \frac{1}{U} \Delta^2 \\ &= \sum_{\mathbf{k}} \begin{bmatrix} c_{\mathbf{k}\uparrow}^\dagger & c_{-\mathbf{k}\downarrow} \end{bmatrix} \begin{bmatrix} \varepsilon_{\mathbf{k}} - \mu & \Delta \\ \Delta & -(\varepsilon_{\mathbf{k}} - \mu) \end{bmatrix} \begin{bmatrix} c_{\mathbf{k}\uparrow} \\ c_{-\mathbf{k}\downarrow} \end{bmatrix} + \sum_{\mathbf{k}} (\varepsilon_{\mathbf{k}} - \mu) + \frac{1}{U} \Delta^2 \\ &= \sum_{\mathbf{k}} \psi_{\mathbf{k}}^\dagger [(\varepsilon_{\mathbf{k}} - \mu) \tau_z + \Delta \tau_x] \psi_{\mathbf{k}} + \sum_{\mathbf{k}} (\varepsilon_{\mathbf{k}} - \mu) + \frac{1}{U} \Delta^2, \end{aligned} \quad (\text{S4})$$

where $\psi_{\mathbf{k}} = \begin{bmatrix} c_{\mathbf{k}\uparrow} \\ c_{-\mathbf{k}\downarrow} \end{bmatrix}$ is the Nambu spinor and $\tau_{x,y,z}$ are Pauli matrices. In the frequency-momentum space, one can directly extract the Gor'kov's Green's function as

$$G(i\omega_n, \mathbf{k}) = \frac{-i\omega_n \tau_0 - (\varepsilon_{\mathbf{k}} - \mu) \tau_z - \Delta \sigma_x}{\omega_n^2 + (\varepsilon_{\mathbf{k}} - \mu)^2 + \Delta^2}, \quad (\text{S5})$$

where $\omega_n = (2n+1)\pi T$ is the Matsubara frequency and τ_0 is a 2×2 identity matrix. With the Gor'kov's Green function in Eq. (S5), we can determine the order parameters by

$$\Delta = -\frac{U}{2N} T \sum_{\mathbf{k}, n} \text{Tr} G(i\omega_n, \mathbf{k}) \tau_x = \frac{U}{N} \sum_{\mathbf{k}, n} \frac{\Delta}{\omega_n^2 + (\varepsilon_{\mathbf{k}} - \mu)^2 + \Delta^2}, \quad (\text{S6})$$

or

$$1 = \frac{U}{N} T \sum_{\mathbf{k}, n} \frac{1}{\omega_n^2 + (\varepsilon_{\mathbf{k}} - \mu)^2 + \Delta^2}. \quad (\text{S7})$$

We also need to determine the chemical potential by the number of equations

$$2\nu = 1 + \frac{T}{N} \sum_{\mathbf{k}, n} \text{Tr} G(i\omega_n, \mathbf{k}) \tau_z. \quad (\text{S8})$$

with ν being the filling factor. Combine Eqs. (S7) and (S8) and we can obtain the superconducting order parameter.

We can evaluate several basic physical quantities in the exact flat-band limit. The zero temperature pairing gap is given by:

$$\Delta_0 = U \sqrt{\nu(1-\nu)} \quad (\text{S9})$$

And the the mean-field transition temperature transition temperature T_c is given by:

$$T_c = \frac{U}{4} \frac{2\nu - 1}{\text{atanh}(2\nu - 1)} = \frac{U}{4} \bar{\nu}. \quad (\text{S10})$$

At half filling, where $\nu = 0.5$, we have $\Delta_0 = 2T_c$, which is different from the conventional BCS relation ($\Delta_0 = 1.76T_c$). If the system has a bandwidth W and in the case of $U \gg W$, We have $\Delta_0 \propto U$ and $T_c \propto U$.

II. GINZBURG LANDAU THEORY FOR SDE

In this section we develop the Ginzburg Landau theory for the superconducting diode effect and consider the quantum geometry effects. The local attractive interaction is given by

$$H_{\text{int}} = -U \int_{\mathbf{r}} d\mathbf{r} a_{+}^{\dagger}(\mathbf{r}) a_{-}^{\dagger}(\mathbf{r}) a_{-}(\mathbf{r}) a_{+}(\mathbf{r}). \quad (\text{S11})$$

with $a_{\sigma}(\mathbf{r})$ as the electron annihilation operator carrying two flavors $\sigma = \pm$. $+$ and $-$ are time-reversal partners. For example, if we consider a two-valley system such as twisted bilayer graphene, $+$ = $\{K, \uparrow\}$ and $-$ = $\{K', \downarrow\}$. U denotes the attractive interaction. We introduce the projection from orbital basis to the band basis, which reads

$$a_{\sigma}(\mathbf{r}) = \frac{1}{\sqrt{N}} \sum_{\mathbf{k}, \alpha} e^{i\mathbf{k} \cdot \mathbf{r}} u_{\alpha\sigma}^*(\mathbf{k}) c_{\mathbf{k}\sigma} \quad (\text{S12})$$

Where α denotes the orbital index. c_{σ} denote the annihilation Fermi operator on the target flat band. Here we have ignored terms containing $u_{\alpha+}(\mathbf{k} + \mathbf{q}) u_{\beta-}(-\mathbf{k})$, which is irrelevant to a superconducting phase. By using the Fourier transform $\Delta(\mathbf{r}) = \sum_{\mathbf{q}} \Delta_{\mathbf{q}} e^{i\mathbf{q} \cdot \mathbf{r}}$, the interaction Hamiltonian can be written as

$$\begin{aligned} H_{\text{int}} &= \sum_{\mathbf{r}} \Delta(\mathbf{r}) a_{+}^{\dagger}(\mathbf{r}) a_{-}^{\dagger}(\mathbf{r}) \\ &= \sum_{\mathbf{k} \mathbf{q} \alpha} u_{\alpha+}(\mathbf{k} + \mathbf{q}) u_{\alpha-}(-\mathbf{k}) \Delta_{\mathbf{q}} c_{\mathbf{k}+\mathbf{q},+}^{\dagger} c_{-\mathbf{k},-}^{\dagger} + h.c. \end{aligned} \quad (\text{S13})$$

Here, $\sum_{\alpha} u_{\alpha+}(\mathbf{k} + \mathbf{q}) u_{\alpha-}(-\mathbf{k}) = \langle u_{\mathbf{k}+\mathbf{q},+} | u_{-\mathbf{k},-}^* \rangle$. Based on this, we can rewrite the interaction Hamiltonian as

$$H_{\text{int}} = \sum_{\mathbf{k}} \Gamma(\mathbf{k}, \mathbf{q}) \Delta_{\mathbf{q}} c_{\mathbf{k}+\mathbf{q},+}^{\dagger} c_{-\mathbf{k},-}^{\dagger} \quad (\text{S14})$$

where $\Gamma(\mathbf{k}, \mathbf{q}) = \langle u_{\mathbf{k}+\mathbf{q},+} | u_{-\mathbf{k},-}^* \rangle$ is the form factor. The next step is to derive the Ginzburg-Landau free energy.

The non-interacting partition function is given by

$$Z = e^{-\beta F} = \text{Tr}[e^{-\beta(H-\mu N)}] \quad (\text{S15})$$

After we consider the electron-electron interaction, the partition function changes to

$$e^{-\beta\delta F} = \frac{\text{Tr}[e^{-\beta(H-\mu N)} e^{-\beta\delta H}]}{\text{Tr}[e^{-\beta(H-\mu N)}]} \quad (\text{S16})$$

The change of the free energy is $\delta F = \delta F_2 + \delta F_4$. The correction to thermodynamic potential due to the interaction is expressed via the average value of S -matrix with $\delta F = -T \ln \langle S \rangle \approx -T(\langle S \rangle - 1)$ where angular brackets denote Gibbs average, while $S = T_\tau \exp[-\int_0^\beta d\tau H_{\text{int}}(\tau)]$.

We can expand $\langle S \rangle - 1$ to

$$\frac{(-1)^n}{n!} \int_0^\beta \dots \int_0^\beta d\tau_1 \dots d\tau_n \langle T_\tau [H_{\text{int}}(\tau_1) \dots H_{\text{int}}(\tau_n)] \rangle \quad (\text{S17})$$

The second order correction to free energy is given by [1]

$$\begin{aligned} \delta F_2 &= -\frac{T}{2} \int_0^\beta d\tau_1 \int_0^\beta d\tau_2 \langle T_\tau (H_{\text{int}}(\tau_1) H_{\text{int}}(\tau_2)) \rangle \\ &= -\frac{T}{2} \int_0^\beta d\tau_1 \int_0^\beta d\tau_2 |\Gamma(\mathbf{k}, \mathbf{q})|^2 \Delta_{\mathbf{q}}^* \Delta_{\mathbf{q}} \left\{ \sum_{\mathbf{k}} G(\mathbf{k} + \mathbf{q}, \tau_1 - \tau_2) G(-\mathbf{k}, \tau_1 - \tau_2) + G(\mathbf{k} + \mathbf{q}, \tau_2 - \tau_1) G(-\mathbf{k}, \tau_2 - \tau_1) \right\} \\ &= -T \int_0^\beta d\tau_1 \int_0^\beta d\tau_2 |\Gamma(\mathbf{k}, \mathbf{q})|^2 |\Delta_{\mathbf{q}}|^2 \sum_{\mathbf{k}} G(\mathbf{k} + \mathbf{q}, \tau_1 - \tau_2) G(-\mathbf{k}, \tau_1 - \tau_2) \end{aligned} \quad (\text{S18})$$

The Green's function $G(\mathbf{k}, \tau_1 - \tau_2) = -\langle T_\tau c_{\mathbf{k}}(\tau_1) c_{\mathbf{k}}^\dagger(\tau_2) \rangle$. After the Fourier transformation, $G(\mathbf{k}, \omega_n) = (i\omega_n - \varepsilon_{\mathbf{k}})^{-1}$.

We can obtain the Ginzburg-Landau coefficients

$$\delta F_2 = -T |\Delta_{\mathbf{q}}|^2 \sum_{\mathbf{k}, n} |\Gamma(\mathbf{k}, \mathbf{q})|^2 G_e(\mathbf{k} + \mathbf{q}, \omega_n) G_h(\mathbf{k}, \omega_n) \quad (\text{S19})$$

$$\delta F_4 = \frac{T}{2} |\Delta_{\mathbf{q}}|^4 \sum_{\mathbf{k}, n} G_e(\mathbf{k}, \omega_n)^2 G_h(\mathbf{k}, \omega_n)^2. \quad (\text{S20})$$

Here $G_e(\mathbf{k}, \omega_n) = (i\omega_n - \varepsilon_{\mathbf{k}+})^{-1}$ and $G_h(\mathbf{k}, \omega_n) = (-i\omega_n - \varepsilon_{-\mathbf{k}-})^{-1}$. The total free energy in the Eq.(5) of main text is written as

$$\Omega = \int d\mathbf{q} (\delta F_2 + \delta F_4) = \int d\mathbf{q} [(a_0 + a_{\mathbf{q}}) |\Delta_{\mathbf{q}}|^2 + \frac{B}{2} |\Delta_{\mathbf{q}}|^4] \quad (\text{S21})$$

Here the $a_{\mathbf{q}} = a_{\mathbf{q}}^c + a_{\mathbf{q}}^g$ includes both the conventional and geometric parts. We can write them as $a_{\mathbf{q}}^c = \frac{\beta_c}{4} (\lambda_c q^2 + \delta_v \alpha_a^{bc} q_a q_b q_c)$ and $a_{\mathbf{q}}^g = \frac{\beta_c}{4} (\bar{\mathcal{G}}_{ab} q_a q_b + \delta_v \bar{\mathcal{D}}_a^{bc} q_a q_b q_c)$. Here δ_v is the time-reversal symmetry breaking term such as valley polarization (we will show later). λ_c is the conventional kinetic energy term which is related to the Fermi velocity v_F . α_a^{bc} is the tensor which describes the Fermi surface asymmetry such as trigonal warping. $\bar{\mathcal{G}}_{ab}$ and $\bar{\mathcal{D}}_a^{bc}$ are the average of quantum metric and quantum metric dipole which are defined in the main text and also in the later section. Because of the rotation symmetry, we have $\bar{\mathcal{G}}_{xx} = \bar{\mathcal{G}}_{yy} \equiv \bar{\mathcal{G}}$ and $\bar{\mathcal{G}}_{xy} = \bar{\mathcal{G}}_{yx} = 0$. Thus we can write down the Cooper pair fluctuation term in the Ginzburg-Landau free energy as

$$a_{\mathbf{q}} = \frac{\beta_c}{4} [(\lambda_c + \bar{\mathcal{G}}) \mathbf{q}^2 + \delta_v (\alpha_a^{bc} + \bar{\mathcal{D}}_a^{bc}) q_a q_b q_c] \quad (\text{S22})$$

Because of C_3 symmetry, $a_{\mathbf{q}}$ should be invariant by changing $\mathbf{q} \rightarrow \mathcal{R}_{2\pi/3} \mathbf{q}$ with \mathcal{R} being the rotation matrix. We further define $\bar{\mathcal{C}}_a^{bc} = \alpha_a^{bc} + \bar{\mathcal{D}}_a^{bc}$. With respect to the C_3 symmetry, we have

$$\bar{\mathcal{C}}_x^{yy} = \bar{\mathcal{C}}_y^{yx} = \bar{\mathcal{C}}_y^{xy} = -\bar{\mathcal{C}}_x^{xx} \quad (\text{S23})$$

$$\bar{\mathcal{C}}_y^{xx} = \bar{\mathcal{C}}_x^{xy} = \bar{\mathcal{C}}_x^{yx} = -\bar{\mathcal{C}}_y^{yy} \quad (\text{S24})$$

Thus the non-equivalent non-zero elements are $\bar{\mathcal{C}}_x^{xx}$ and $\bar{\mathcal{C}}_y^{yy}$. We have

$$\sum_{abc} \bar{\mathcal{C}}_a^{bc} q_a q_b q_c = \bar{\mathcal{C}}_x^{xx} (q_x^3 - 3q_x q_y^2) + \bar{\mathcal{C}}_y^{yy} (q_y^3 - 3q_y q_x^2) = \bar{\mathcal{C}}_x^{xx} \cos 3\theta - \bar{\mathcal{C}}_y^{yy} \sin 3\theta \quad (\text{S25})$$

A. Conventional contributions

We derive the Ginzburg-Landau coefficients for the case of the narrow band with finite bandwidth W and the interaction strength $U \gtrsim W$. In this case, we have $\beta_c W \lesssim 1$. $\beta_c = 1/T_c$ with T_c being the mean field transition temperature. We set the Fermi energy $\mu = 0$ and thus $\varepsilon_{\mathbf{k}} \in [-W/2, W/2]$. The δ_v is the interaction-driven valley polarization, which breaks \mathcal{T} and can be introduced as $\varepsilon_{\mathbf{k}\sigma} \rightarrow \varepsilon_{\mathbf{k}\sigma} + \sigma\delta_v$. Firstly, we derive the \mathbf{q} -independent terms a_0 and B . We have

$$\begin{aligned}
a_0 &= \frac{1}{U} - T \sum_{\mathbf{k}, n} G_e(\mathbf{k}, \omega_n) G_h(\mathbf{k}, \omega_n) \\
&= \frac{1}{U} - \sum_{\mathbf{k}} \frac{\tanh(\frac{\beta \varepsilon_{\mathbf{k}}}{2})}{2\varepsilon_{\mathbf{k}}} \\
&= \sum_{\mathbf{k}} \frac{\tanh(\frac{\beta_c \varepsilon_{\mathbf{k}}}{2})}{2\varepsilon_{\mathbf{k}}} - \sum_{\mathbf{k}} \frac{\tanh(\frac{\beta \varepsilon_{\mathbf{k}}}{2})}{2\varepsilon_{\mathbf{k}}} \\
&\approx \frac{1}{W} \tanh \frac{\beta_c W}{4} \frac{T - T_c}{T_c},
\end{aligned} \tag{S26}$$

and

$$\begin{aligned}
B &= T_c \sum_{\mathbf{k}, n} G_e^2(\mathbf{k}, \omega_n) G_h^2(\mathbf{k}, \omega_n) \\
&\approx \frac{\beta_c}{2W^3} (W - \frac{4}{\beta_c} \tanh \frac{\beta_c W}{4}).
\end{aligned} \tag{S27}$$

In the above derivations we keep the leading order for $\beta_c W \lesssim 1$ and the density of states $\rho \approx 1/W$. In the limit $\beta_c W \rightarrow 0$, we have $a_0 = \beta_c(T - T_c)/(4T_c)$ and $B = \beta_c^3/96$. Secondly, the Cooper pair fluctuation term a_q can be divided in to the conventional term a_q^c and the geometric term a_q^g , with $a_q = a_q^c + a_q^g$. We first derive a_q^c , which reads

$$\begin{aligned}
a_q^c &= -T_c \sum_{\mathbf{k}, n} [G_e(\mathbf{k} + \mathbf{q}, \omega_n) G_h(\mathbf{k}, \omega_n) - G_e(\mathbf{k}, \omega_n) G_h(\mathbf{k}, \omega_n)] \\
&\approx -T_c \sum_{\mathbf{k}, n} G_h [\mathbf{q} \cdot \nabla_{\mathbf{k}} + \frac{1}{2} (\mathbf{q} \cdot \nabla_{\mathbf{k}})^2 + \frac{1}{6} (\mathbf{q} \cdot \nabla_{\mathbf{k}})^3] G_e
\end{aligned} \tag{S28}$$

Here we use the notations that $G_e = G_e(\mathbf{k}, \omega_n)$ and $G_h = G_h(\mathbf{k}, \omega_n)$. $\nabla_{\mathbf{k}}$ is the derivative of the wave number. The first-order term is zero due to the rotational symmetry. The second-order term is

$$-T_c \sum_{\mathbf{k}, n} \frac{1}{2} G_h (\mathbf{q} \cdot \nabla_{\mathbf{k}})^2 G_e = \frac{T_c}{2} \sum_{\mathbf{k}, n} (\mathbf{q} \cdot \nabla_{\mathbf{k}} G_h) (\mathbf{q} \cdot \nabla_{\mathbf{k}} G_e) = \frac{T_c}{2} \sum_{\mathbf{k}, n} q_a q_b v_a v_b G_h^2 G_e^2 \tag{S29}$$

Thus we can obtain

$$\lambda_c = 2T_c^2 \sum_{\mathbf{k}, n} v_x^2 G_h^2 G_e^2 \tag{S30}$$

Here $v_a = \partial_{k_a} \varepsilon_{\mathbf{k}}$. The third-order term can be derived as

$$\begin{aligned}
-T_c \sum_{\mathbf{k}, n} \frac{1}{6} G_h (\mathbf{q} \cdot \nabla_{\mathbf{k}})^3 G_e &= -T_c \sum_{\mathbf{k}, n} G_h q_a q_b a_c (\frac{1}{6} v_{abc} G_e^2 + v_{ab} v_c G_e^3 + v_a v_b v_c G_e^4) \\
&= -\delta_v T_c \sum_{\mathbf{k}, n} q_a q_b a_c [\frac{1}{6} v_{abc} (2G_e^3 G_h - G_e^2 G_h^2) + v_{ab} v_c (3G_e^4 G_h - G_e^3 G_h^2) + v_a v_b v_c (4G_e^5 G_h - G_e^4 G_h^2)].
\end{aligned} \tag{S31}$$

Here $v_{abc} = \partial^3 \varepsilon_{\mathbf{k}} / \partial k_a \partial k_b \partial k_c$ and $v_{ab} = \partial^2 \varepsilon_{\mathbf{k}} / \partial k_a \partial k_b$. Thus we can obtain

$$\alpha_a^{bc} = -4T_c^2 \sum_{\mathbf{k}, n} [\frac{1}{6} v_{abc} (2G_e^3 G_h - G_e^2 G_h^2) + v_{ab} v_c (3G_e^4 G_h - G_e^3 G_h^2) + v_a v_b v_c (4G_e^5 G_h - G_e^4 G_h^2)] \tag{S32}$$

The Eq. (30), Eq. (32) can be used to calculate the conventional contributions for arbitrary model Hamiltonian. α_a^{bc} is the tensor for Fermi surface asymmetry. For C_3 symmetric systems, the non-equivalent non-zero elements are α_x^{xx} and α_y^{yy} .

Clearly, in the limit of $\beta_c W \rightarrow 0$, $\sum_n 2G_e^3 G_h - G_e^2 G_h^2 = -\frac{1}{16}\beta_c^4 + \mathcal{O}(\beta_c^6)$, $\sum_n 3G_e^4 G_h - G_e^3 G_h^2 = \frac{1}{48}\varepsilon_{\mathbf{k}}\beta_c^6 + \mathcal{O}(\beta_c^8)$, and $\sum_n 4G_e^5 G_h - G_e^4 G_h^2 = \frac{1}{96}\beta_c^6 + \mathcal{O}(\beta_c^8)$. By keeping the leading order, $\alpha_a^{bc} \rightarrow \frac{\beta_c^2}{24}\sum_{\mathbf{k}} v_{abc} + \mathcal{O}(\beta_c^4)$ in the limit of $\beta_c W \rightarrow 0$. With the periodic boundary condition, $\sum_{\mathbf{k}} v_{abc} = 0$ and α_a^{bc} scales as β_c^4 . We also have $\lambda_c \sim (\beta_c W)^2$.

B. Geometric contributions

We now drive the geometric part in the Ginzburg-Landau coefficients. We can write the $a_{\mathbf{q}}^g$ as the sum of second order and third order terms as $a_{\mathbf{q}}^g = a_{\mathbf{q}}^{g,2} + a_{\mathbf{q}}^{g,3}$. From Eq.(19), we have

$$a_{\mathbf{q}}^g = T_c \sum_{\mathbf{k}, n} (1 - |\Gamma(\mathbf{k}, \mathbf{q})|^2) G_e(\mathbf{k} + \mathbf{q}, \omega_n) G_h(\mathbf{k}, \omega_n). \quad (\text{S33})$$

Here the $|\Gamma(\mathbf{k}, \mathbf{q})|$ is the form factor and can be expanded as

$$|\Gamma(\mathbf{k}, \mathbf{q})|^2 = |\langle u_{\mathbf{k}+\mathbf{q}} | u_{\mathbf{k}} \rangle|^2 = 1 - \mathcal{G}_{ab} q_a q_b + \mathcal{O}(q^3) \quad (\text{S34})$$

Based on this, we can derive that

$$\begin{aligned} a_{\mathbf{q}}^g &= T_c \sum_{\mathbf{k}, n} \mathcal{G}_{ab} q_a q_b G_e(\mathbf{k} + \mathbf{q}, \omega_n) G_h(\mathbf{k}, \omega_n) \\ &= T_c \sum_{\mathbf{k}, n} \mathcal{G}_{ab} q_a q_b [G_e(\mathbf{k}, \omega_n) G_h(\mathbf{k}, \omega_n) + q_c v_c(\mathbf{k}) G_e^2(\mathbf{k}, \omega_n) G_h(\mathbf{k}, \omega_n)] \end{aligned} \quad (\text{S35})$$

By integrating the left part in Eq. (35), we further have

$$a_{\mathbf{q}}^{g,2} = \frac{\beta_c}{4} \sum_{\mathbf{k}} \mathcal{G}_{ab} \frac{\tanh(\beta_c \varepsilon_{\mathbf{k}}/2)}{\beta_c \varepsilon_{\mathbf{k}}/2} q_a q_b = \frac{\beta_c}{4} \bar{\mathcal{G}}_{ab} q_a q_b \quad (\text{S36})$$

The q^3 term can be derived as

$$\begin{aligned} a_{\mathbf{q}}^{g,3} &= -\delta_v \sum_{\mathbf{k}} v_a(\mathbf{k}) \mathcal{G}_{bc}(\mathbf{k}) q_a q_b q_c \frac{\text{sech}^2(\beta_c \varepsilon_{\mathbf{k}}/2) \tanh(\beta_c \varepsilon_{\mathbf{k}}/2)}{8 \varepsilon_{\mathbf{k}}} \beta_c^2 \\ &= \frac{\beta_c^2}{4} \delta_v \sum_{\mathbf{k}} v_a(\mathbf{k}) \mathcal{G}_{bc}(\mathbf{k}) q_a q_b q_c f'_\varepsilon \frac{\tanh(\beta_c \varepsilon_{\mathbf{k}}/2)}{\beta_c \varepsilon_{\mathbf{k}}/2} \end{aligned} \quad (\text{S37})$$

We can use $a_{\mathbf{q}}^g = \frac{\beta_c}{4} \sqrt{\det(\bar{\mathcal{G}}_{ab})} q^2 + \frac{\beta_c}{4} \bar{\mathcal{D}}_a^{bc} q_a q_b q_c$ by defining:

$$\bar{\mathcal{G}}_{ab} = \sum_{\mathbf{k}} \mathcal{G}_{ab}(\mathbf{k}) \frac{\tanh(\beta_c \varepsilon_{\mathbf{k}}/2)}{\beta_c \varepsilon_{\mathbf{k}}/2} \quad (\text{S38})$$

$$\bar{\mathcal{D}}_a^{bc} = \beta_c \sum_{\mathbf{k}} v_a(\mathbf{k}) \mathcal{G}_{bc}(\mathbf{k}) f'_\varepsilon \frac{\tanh(\beta_c \varepsilon_{\mathbf{k}}/2)}{\beta_c \varepsilon_{\mathbf{k}}/2} \quad (\text{S39})$$

In the limit $\beta_c W \rightarrow 0$, we have

$$\bar{\mathcal{G}}_{ab} = \sum_{\mathbf{k}} \mathcal{G}_{ab}(\mathbf{k}) \quad (\text{S40})$$

$$\bar{\mathcal{D}}_a^{bc} = -\frac{\beta_c^2}{4} \sum_{\mathbf{k}} v_a(\mathbf{k}) \mathcal{G}_{bc}(\mathbf{k}) \quad (\text{S41})$$

In this limit, the quantum geometry becomes the leading order.

Supplementary Table 1. The summary of the scaling behaviors for GL coefficient. Here $\beta_c \propto 1/U$.

	λ_c	α	$\bar{\mathcal{G}}$	$\bar{\mathcal{D}}$
$\beta_c W \gg 1$	β_c	β_c^3	$\beta_c^{-1} \ln \beta_c$	β_c
$\beta_c W \ll 1$	β_c^2	β_c^4	β_c^0	β_c^2

For the conventional BCS superconductors, we have the limit of $\beta_c W \rightarrow \infty$. In this case, the Ginzburg-Landau coefficients have different scaling behaviors. For the geometric terms, we have

$$\begin{aligned}
\bar{\mathcal{G}}_{ab} &= 4T_c^2 \sum_{\mathbf{k}, n} \mathcal{G}_{ab} G_e G_h = 4T_c^2 \rho_\epsilon \tilde{\mathcal{G}}_{ab} \pi \sum_n \frac{1}{|\omega_n|} = 4T_c^2 \rho_\epsilon \tilde{\mathcal{G}}_{ab} \pi \sum_{\omega_n < \Lambda} \frac{1}{|\omega_n|} \\
&\approx 4T_c \rho_\epsilon \tilde{\mathcal{G}}_{ab} \int_{1/\beta}^\Lambda \frac{1}{\omega} d\omega \\
&= 4\tilde{\mathcal{G}}_{ab} \rho_\epsilon \beta_c^{-1} \ln(\beta_c \Lambda) \sim \beta_c^{-1} \ln \beta_c
\end{aligned} \tag{S42}$$

Here $\tilde{\mathcal{G}}_{ab}$ is the average of quantum metric on the Fermi surface, which can be expressed as $\tilde{\mathcal{G}}_{ab} = \oint \mathcal{G}_{ab}(\mathbf{k}_F) d\mathbf{k}_F$ with \mathbf{k}_F being the wave vector on the Fermi surface. ρ_ϵ is the density of states on the Fermi surface and Λ is the cutoff of bandwidth. The quantum metric dipole term can be evaluated as

$$\begin{aligned}
\bar{\mathcal{D}}_a^{bc} &= 4T_c^2 \sum_{n\mathbf{k}} v_a \mathcal{G}_{bc} (2G_e^3 G_h - G_e^2 G_h^2) \\
&= 4\pi T_c^2 \bar{d}_a^{bc} \rho_\epsilon \sum_n -\frac{1}{|\omega_n^3|} \\
&= -7\beta_c \bar{d}_a^{bc} \rho_\epsilon \zeta(3) / \pi^2 \sim \beta_c
\end{aligned} \tag{S43}$$

Here \bar{d}_a^{bc} is the average of quantum metric dipole on the Fermi surface, which can be expressed as $\bar{d}_a^{bc} = \oint d_a^{bc}(\mathbf{k}_F) d\mathbf{k}_F$. For the conventional terms, we have $\lambda_c \sim \beta_c$ and $\alpha \sim \beta_c^3$ [2]. The scaling behaviors of the GL coefficient for the conventional limit ($\beta_c W \gg 1$) and the flat-band limit ($\beta_c W \ll 1$) are listed in Table. 1. We summarize the GL coefficient that

$$\lambda_c = 2T_c^2 \sum_{\mathbf{k}, n} v_x^2 G_h^2 G_e^2 \tag{S44}$$

$$\alpha_a^{bc} = -4T_c^2 \sum_{\mathbf{k}, n} \left[\frac{1}{6} v_{abc} (2G_e^3 G_h - G_e^2 G_h^2) + v_{ab} v_c (3G_e^4 G_h - G_e^3 G_h^2) + v_a v_b v_c (4G_e^5 G_h - G_e^4 G_h^2) \right] \tag{S45}$$

$$\bar{\mathcal{G}}_{ab} = \sum_{\mathbf{k}} \mathcal{G}_{ab}(\mathbf{k}) \frac{\tanh(\beta_c \epsilon_{\mathbf{k}}/2)}{\beta_c \epsilon_{\mathbf{k}}/2} \tag{S46}$$

$$\bar{\mathcal{D}}_a^{bc} = -\beta_c \sum_{\mathbf{k}} \partial_a [\mathcal{G}_{bc}(\mathbf{k}) \frac{\tanh(\beta_c \epsilon_{\mathbf{k}}/2)}{\beta_c \epsilon_{\mathbf{k}}/2}] f_{\epsilon_{\mathbf{k}}} \tag{S47}$$

Here the quantum metric dipole term has been renormalized after the integration by part. These formulas can be used to calculate the Ginzburg-Landau coefficients for a concrete model Hamiltonian.

III. SELF-CONSISTENT MEAN-FIELD STUDY OF SUPERCURRENT

In multi-orbital superconductors, in general we have multi order parameters, which need to be optimized self-consistently at the same time. However, in the case of we have narrow bands near Fermi energy, we can simplify the system by changing from orbital basis to the band basis and project the interaction on to the target flat band. In this section, we provide an band-projection method to study the supercurrent by assuming the attractive interaction is within the single flat band. This method is not a strict handling, but it can capture the main physics and divide the geometric supercurrent from the total one. We start with a multi-band Hamiltonian that can be divided into two components: the non-interacting part which is denoted as H_0 and the attractive interaction part which is represented by H_{int} . The total Hamiltonian is $H = H_0 + H_{\text{int}}$ with

$$H_{\text{int}} = -U \int_{\mathbf{r}} d\mathbf{r} a_+^\dagger(\mathbf{r}) a_-^\dagger(\mathbf{r}) a_-(\mathbf{r}) a_+(\mathbf{r}). \tag{S48}$$

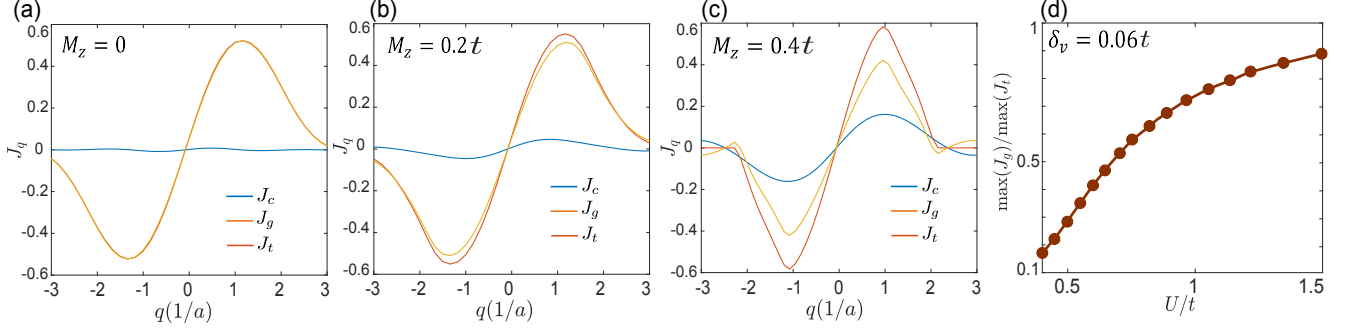


FIG. S1. (a)-(c) The q dependence of the supercurrent for different M_z with $\delta_v = 0$. J_c , J_g , J_t denote the supercurrent from conventional band dispersion, quantum geometry and the total one, respectively. (d) The ratio of $\max(J_g)$ and $\max(J_t)$ as a function of U at $\delta_v = 0.06t$ and $M_z = 0.5t$.

Here, with the mean-field decoupling, we can write H_{int} as

$$H_{\text{int}} = \int_{\mathbf{r}} d\mathbf{r} \Delta(\mathbf{r}) a_{+}^{\dagger}(\mathbf{r}) a_{-}^{\dagger}(\mathbf{r}) + \frac{|\Delta(\mathbf{r})|^2}{2U}. \quad (\text{S49})$$

After the Fourier transformation, we have

$$\begin{aligned} H_{\text{int}} &= \sum_{\mathbf{q}, \mathbf{k}, \alpha} \Delta(\mathbf{q}) u_{\alpha+}(\mathbf{k} + \mathbf{q}) u_{\alpha-}(-\mathbf{k}) c_{+}^{\dagger}(\mathbf{k} + \mathbf{q}) c_{-}^{\dagger}(-\mathbf{k}) + \frac{|\Delta(\mathbf{q})|^2}{2U} \\ &= \sum_{\mathbf{q}, \mathbf{k}} \Delta(\mathbf{q}) \Gamma(\mathbf{k}, \mathbf{q}) c_{+}^{\dagger}(\mathbf{k} + \mathbf{q}) c_{-}^{\dagger}(-\mathbf{k}) + \frac{|\Delta(\mathbf{q})|^2}{2U} \end{aligned} \quad (\text{S50})$$

The form factor Γ emerges from the product of the Bloch states $\Gamma(\mathbf{k}, \mathbf{q}) = \sum_{\alpha} u_{\alpha}(\mathbf{k} + \mathbf{q}) u_{\alpha}^{*}(\mathbf{k})$, where we assume a time-reversal symmetry $u_{\alpha}(\mathbf{k}) \equiv u_{\alpha+}(\mathbf{k}) = u_{\alpha-}^{*}(-\mathbf{k})$. Physically, this projection is valid, as we anticipate the emergence of superconducting pairing order exclusively within the isolated band. The single band Hamiltonian with spin degeneracy is given by

$$H_0 \rightarrow \sum_{\mathbf{k}} \varepsilon_{\sigma}(\mathbf{k}) c_{\sigma}^{\dagger}(\mathbf{k}) c_{\sigma}(\mathbf{k}). \quad (\text{S51})$$

By including the pairing potential $\Delta(\mathbf{q})$, the Bogoliubov-de Gennes (BdG) Hamiltonian can be written as

$$H_{\text{BdG}}(\mathbf{k}, \mathbf{q}) = \begin{pmatrix} \varepsilon_{+}(\mathbf{k} + \mathbf{q}) - \mu + \delta_v & \Delta(\mathbf{q}) \Gamma(\mathbf{k}, \mathbf{q}) \\ \Delta(\mathbf{q}) \Gamma^{*}(\mathbf{k}, \mathbf{q}) & -\varepsilon_{-}(-\mathbf{k}) + \mu + \delta_v \end{pmatrix} \quad (\text{S52})$$

Here δ_v is the valley polarization which breaks the time-reversal symmetry. Thus The total free energy can be written as

$$F(\mathbf{q}) = -\frac{1}{2\beta} \sum_{\mathbf{k}, n} \ln[1 + e^{-\beta E_n(\mathbf{k}, \mathbf{q})}] + \frac{|\Delta(\mathbf{q})|^2}{2U} \quad (\text{S53})$$

Here $E_n(\mathbf{k}, \mathbf{q})$ is the eigenvalues of H_{BdG} . $n = 1, 2$ is for the electron and hole band, respectively. By minimize the free energy by $\partial F/\partial \Delta = 0$, we can obtain the self-consistent solution for $\Delta(\mathbf{q})$:

$$1 = -U \sum_{\mathbf{k}} |\Gamma(\mathbf{k}, \mathbf{q})|^2 \frac{\tanh[\beta E(\mathbf{k}, \mathbf{q})/2]}{2E(\mathbf{k}, \mathbf{q})} \quad (\text{S54})$$

Here $E(\mathbf{k}, \mathbf{q}) = E_1(\mathbf{k}, \mathbf{q})$ is the quasiparticle energy. The total supercurrent can be derived as $J_{\mathbf{q}} = 2\partial_{\mathbf{q}} F(\mathbf{q})$. The conventional supercurrent can be obtained with $\Gamma = 1$.

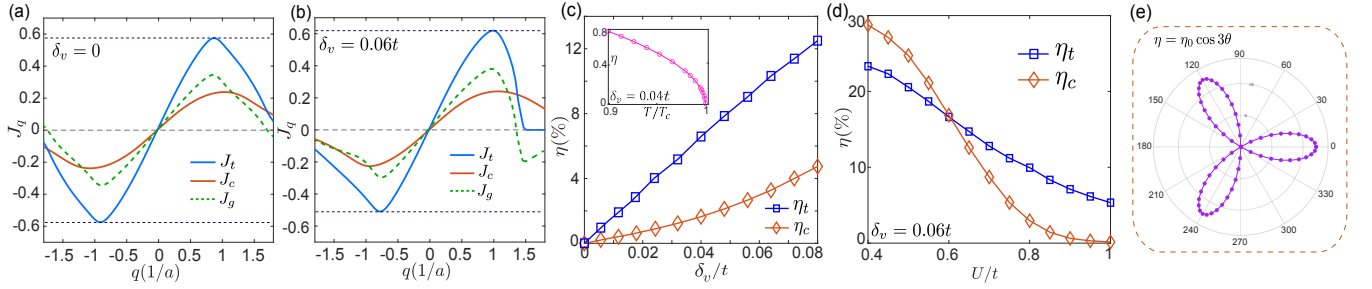


FIG. S2. (a) The q dependence of the supercurrent J_q without valley polarization δ_v . The total and conventional currents, denoted as J_t and J_c , are plotted in blue and orange lines, respectively. The current from quantum geometry (J_g) is plotted in the green dashed line. In this case, there is no diode effect. (b) The q dependence of the J_q at $\delta_v = 0.06t$. In this case, J_t , J_c and J_g all exhibit nonreciprocal behaviors. (c) The diode quality factors of total current η_t and conventional current η_c as a function of δ_v . The inset shows the temperature dependence of η_t near T_c at $\delta_v = 0.04t$. (d) η_c and η_t as a function of U . (e) The angular dependence of η with $\eta = \eta_0 \cos 3\theta$ and $\eta_0 = 12\%$ at $\delta_v = 0.08t$ and $U = 0.8t$. Parameters: for all five panels, $\mu = -2.15t$, $T = 0.02t$, $M_z = 0.5t$.

We present a mean-field study for a flattened Haldane-like model with two valleys and two orbitals (A and B) per-site on the triangular lattice [3]. The real-space Hamiltonian has the form

$$h_0^\sigma = - \sum_{\langle ij \rangle} t a_{i\sigma}^\dagger b_{j\sigma} - \sum_{\langle ij \rangle'} t_A^\sigma a_{i\sigma}^\dagger a_{j\sigma} + t_B^\sigma b_{i\sigma}^\dagger b_{j\sigma} - \sum_{\langle ij \rangle''} t_3 a_{i\sigma}^\dagger b_{j\sigma} + \sum_i M_z (a_{i\sigma}^\dagger a_{i\sigma} - b_{i\sigma}^\dagger b_{i\sigma}), \quad (\text{S55})$$

where $\sigma = \pm 1$ denotes the valley, and operator $a(b)_{i\sigma}$ annihilates a fermion with σ valley in the orbital $A(B)$ on site i . $\langle ij \rangle$ represents the first-nearest hopping term with magnitude t . M_z is the mass term on the A and B orbitals. The second-neighbor hopping terms are denoted by t_A^σ and t_B^σ , with $t_X^- = (t_X^+)^*$ due to \mathcal{T} symmetry. Specifically, we set $t_A^+ = t_2 e^{i\pi/2}$ and $t_B^+ = t_2 e^{-i\pi/2}$. The notation $\langle ij \rangle''$ refers to the third-nearest hopping. The other parameters are chosen as $t_2 = 0.39t$ and $t_3 = -0.34t$. The Hamiltonian in momentum space is $h_0^+ = h_x \sigma_x + h_y \sigma_y + (h_z + M_z) \sigma_z$. We have

$$h_x = -t_1 [\cos(k_1) + \cos(k_2) + \cos(k_1 - k_2)] - t_3 [\cos(2k_1) + \cos(2k_2) + \cos(2k_1 - 2k_2)] \quad (\text{S56})$$

$$h_y = t_1 [\sin(k_1) - \sin(k_2) - \sin(k_1 - k_2)] - t_3 [\sin(2k_1) - \sin(2k_2) - \sin(2k_1 - 2k_2)] \quad (\text{S57})$$

$$h_z = -2t_2 [\sin(k_1 - 2k_2) - \sin(2k_1 - k_2) + \sin(k_1 + k_2)] \quad (\text{S58})$$

with $k_1 = k_y/2 + \sqrt{3}k_x/2$ and $k_2 = -k_y/2 + \sqrt{3}k_x/2$. The time-reversal partner $h_0^-(\mathbf{k}) = h_0^{+*}(-\mathbf{k})$.

We adopt the band-projection method to study the supercurrent where the Fermi energy lies on the lower band. The supercurrent from conventional band dispersion (J_c) and the total one (J_t) incorporated with the quantum geometry can be computed directly, while the geometric contribution is approximately $J_g \approx J_t - J_c$. In Fig.S1 we show the calculation of the supercurrent as a function of $\mathbf{q} = q\hat{x}$ for different M_z . We set $U = 0.8t$ and $\mu = -2.15t$. When $M_z = 0$, the bandwidth is nearly zero and thus the supercurrent from conventional part is very small. As M_z gets larger, it is clear that the supercurrent from conventional part gets larger because of the enlarged bandwidth. In the main text, we already show that the supercurrent is dominated by the geometric part in the large U case. In Fig.S1 (f) we show the U dependence of the ratio of $\max(J_g)$ and $\max(J_t)$. As U increases, it approaches to 1 indicating that the geometric supercurrent dominates in the large U regime. This behavior is consistent with Ginzburg-Landau analysis.

Next we study the diode effect by introducing the valley polarization δ_v . In Fig. S2 (a) there is no diode effect because $\delta_v = 0$ to preserve the \mathcal{T} symmetry. In Fig. S2 (b), the diode effect shows up for finite δ_v . Obviously, besides the J_c and J_t , the J_g is also nonreciprocal arising from the quantum metric dipole. In Fig. S2 (c) we find that the diode quality factor η grows linearly for small δ_v in both the total (η_t) and conventional (η_c) cases. The inset reveals the temperature scaling of η as $\sqrt{T_c - T}$ near T_c . In Fig. S2 (d) we show the U dependence of η_c and η_t . As U increases, η_c decays faster than η_t and $\eta_t \gg \eta_c$ when U is large, indicating that the quantum geometry dominates in the large U regime. Since the geometric supercurrent can not be calculated directly, it can be inferred that the quantum metric dipole plays a pivotal role for the SDE in the large U regime, which is consistent with the Ginzburg-Landau analysis. We also show the angular dependence of η in Fig. S2 (e) by using $\mathbf{q} = q(\cos \theta, \sin \theta)$ and verify that $\eta \sim \cos(3\theta)$.

IV. APPLICATION TO MOIRÉ SUPERCONDUCTORS

A. Continuum model of moiré graphene

In this section, we provide the calculations of the band structure by using the continuum model for twisted bilayer graphene (TBG) and twisted trilayer graphene (TTG) [4]. The TBG is formed by two layers with a twist angle $-\theta/2$ and $\theta/2$ relative to x axis respectively. In the continuum limit by neglecting the intervalley mixing, the Hamiltonian reads:

$$H = H_1 + H_2 + H_{int} \quad (\text{S59})$$

Here, $H_{1/2}$ denotes the Hamiltonian of the top/bottom layer, and H_{int} denotes the interlayer coupling. $H_{1/2}$ reads:

$$H_1 = \sum_{\xi, \mathbf{k}} a_{1, \xi, \mathbf{k}}^\dagger \hbar v_F \hat{R}_{\theta/2}(\mathbf{k} - \mathbf{K}_1) \cdot (\xi \sigma_x, \sigma_y) a_{1, \xi, \mathbf{k}} \quad (\text{S60})$$

$$H_2 = \sum_{\xi, \mathbf{k}} a_{2, \xi, \mathbf{k}}^\dagger \hbar v_F \hat{R}_{-\theta/2}(\mathbf{k} - \mathbf{K}_2) \cdot (\xi \sigma_x, \sigma_y) a_{2, \xi, \mathbf{k}} \quad (\text{S61})$$

where $\hat{R}_\theta = \begin{pmatrix} \cos \theta & -\sin \theta \\ \sin \theta & \cos \theta \end{pmatrix}$ is the rotation operator. σ acts on the spinor of sublattices A and B in graphene. $\xi = \pm$ denotes the K and K' valleys. The interlayer coupling can be written as

$$H_{int} = \sum_{\xi} \int_{\mathbf{r}} \psi_{1, \xi}^\dagger(\mathbf{r}) T(\mathbf{r}) \psi_{2, \xi}(\mathbf{r}) + h.c. \quad (\text{S62})$$

where

$$T(\mathbf{r}) = \begin{pmatrix} w_0 & w_1 \\ w_1 & w_0 \end{pmatrix} + \begin{pmatrix} w_0 & w_1 e^{-i\frac{2\pi}{3}} \\ w_1 e^{i\frac{2\pi}{3}} & w_0 \end{pmatrix} e^{-i\mathbf{G}_1^M \cdot \mathbf{r}} + \begin{pmatrix} w_0 & w_1 e^{i\frac{2\pi}{3}} \\ w_1 e^{-i\frac{2\pi}{3}} & w_0 \end{pmatrix} e^{-i(\mathbf{G}_1^M + \mathbf{G}_2^M) \cdot \mathbf{r}} \quad (\text{S63})$$

With the relation $\psi_{i, \xi}(\mathbf{r}) = \sum_{\mathbf{k}} a_{i, \xi, \mathbf{k}} e^{i\mathbf{k} \cdot \mathbf{r}}$, the interlayer coupling can be expressed as

$$H_{int} = \sum_{\xi} a_{1, \xi, \mathbf{k}}^\dagger \left[\begin{pmatrix} w_0 & w_1 \\ w_1 & w_0 \end{pmatrix} \delta_{\mathbf{k}, \mathbf{k}'} + \begin{pmatrix} w_0 & w_1 e^{-i\frac{2\pi}{3}} \\ w_1 e^{i\frac{2\pi}{3}} & w_0 \end{pmatrix} \delta_{\mathbf{k} + \mathbf{G}_1^M, \mathbf{k}'} + \begin{pmatrix} w_0 & w_1 e^{i\frac{2\pi}{3}} \\ w_1 e^{-i\frac{2\pi}{3}} & w_0 \end{pmatrix} \delta_{\mathbf{k} + \mathbf{G}_1^M + \mathbf{G}_2^M, \mathbf{k}'} \right] a_{2, \xi, \mathbf{k}'} + h.c. \quad (\text{S64})$$

We adopt the parameters with $\hbar v_F = 5252.44 \text{ meV} \cdot \text{\AA}$, $w_0 = 79.7 \text{ meV}$ and $w_1 = 97.5 \text{ meV}$.

For TTG, the moiré pattern is formed by the rotation of the top and bottom layer with angle $-\theta/2$ and the middle layer with angle $\theta/2$ relative to x axis respectively. For TTG, the Hamiltonian reads

$$H = H_t + H_m + H_b + H_{int}^{tm} + H_{int}^{bm}. \quad (\text{S65})$$

Here $H_{t,m,b}$ denote the Hamiltonian of the top, middle, and bottom layers, respectively. H_{int}^{tm} is the interlayer coupling of the top and middle layers and H_{int}^{bm} is the interlayer coupling of the bottom and middle layers. $H_{t,m,b}$ reads:

$$H_t = \sum_{\xi, \mathbf{k}} a_{t, \xi, \mathbf{k}}^\dagger \hbar v_F \hat{R}_{\theta/2}(\mathbf{k} - \mathbf{K}_1) \cdot (\xi \sigma_x, \sigma_y) a_{t, \xi, \mathbf{k}} \quad (\text{S66})$$

$$H_m = \sum_{\xi, \mathbf{k}} a_{m, \xi, \mathbf{k}}^\dagger \hbar v_F \hat{R}_{-\theta/2}(\mathbf{k} - \mathbf{K}_2) \cdot (\xi \sigma_x, \sigma_y) a_{m, \xi, \mathbf{k}} \quad (\text{S67})$$

$$H_b = \sum_{\xi, \mathbf{k}} a_{b, \xi, \mathbf{k}}^\dagger \hbar v_F \hat{R}_{\theta/2}(\mathbf{k} - \mathbf{K}_1) \cdot (\xi \sigma_x, \sigma_y) a_{b, \xi, \mathbf{k}}, \quad (\text{S68})$$

and

$$H_{int}^{tm} = \sum_{\xi} a_{t, \xi, \mathbf{k}}^\dagger \left[\begin{pmatrix} w_0 & w_1 \\ w_1 & w_0 \end{pmatrix} \delta_{\mathbf{k}, \mathbf{k}'} + \begin{pmatrix} w_0 & w_1 e^{-i\frac{2\pi}{3}} \\ w_1 e^{i\frac{2\pi}{3}} & w_0 \end{pmatrix} \delta_{\mathbf{k} + \mathbf{G}_1^M, \mathbf{k}'} + \begin{pmatrix} w_0 & w_1 e^{i\frac{2\pi}{3}} \\ w_1 e^{-i\frac{2\pi}{3}} & w_0 \end{pmatrix} \delta_{\mathbf{k} + \mathbf{G}_1^M + \mathbf{G}_2^M, \mathbf{k}'} \right] a_{m, \xi, \mathbf{k}'} + h.c. \quad (\text{S69})$$

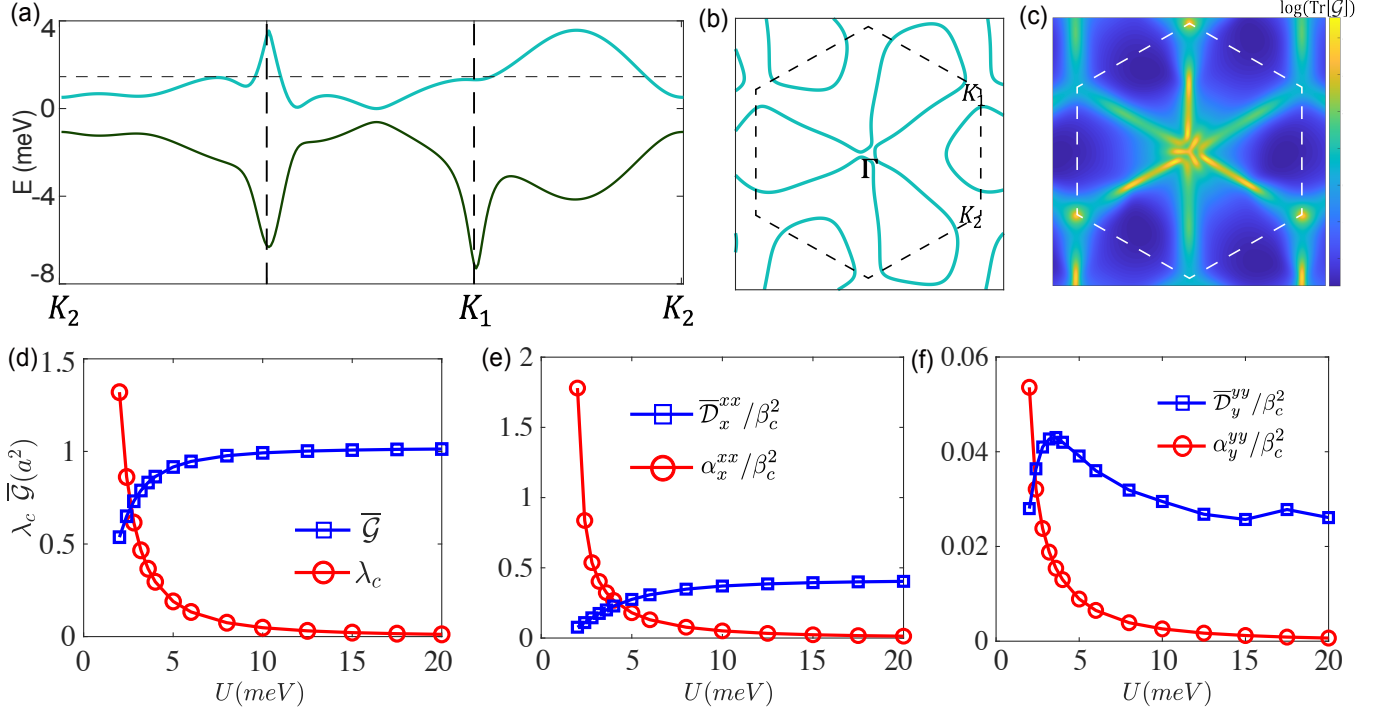


FIG. S3. (a) The band structure of TTBG at $\theta = 1.3^\circ$. The finite layer potential is applied as $V_z = 50$ meV. The half-filling of the lowest conduction band is at $\mu = 1.8$ meV, which is labeled by dashed line at the Fermi surface is plotted in (b). (c) The quantum metric of the conduction band in (a). (d) The calculated $\lambda_c, \bar{\mathcal{G}}$ as a function of interaction strength U . (e) The calculated $\alpha_x^{xx}, \bar{\mathcal{D}}_x^{xx}$ as a function of U . (f) The same as in (e) for α_y^{yy} and $\bar{\mathcal{D}}_y^{yy}$.

$$H_{int}^{bm} = \sum_{\xi} a_{b,\xi,\mathbf{k}}^{\dagger} \left[\begin{pmatrix} w_0 & w_1 \\ w_1 & w_0 \end{pmatrix} \delta_{\mathbf{k},\mathbf{k}'} + \begin{pmatrix} w_0 & w_1 e^{-i\frac{2\pi}{3}} \\ w_1 e^{i\frac{2\pi}{3}} & w_0 \end{pmatrix} \delta_{\mathbf{k}+\mathbf{G}_1^M,\mathbf{k}'} + \begin{pmatrix} w_0 & w_1 e^{i\frac{2\pi}{3}} \\ w_1 e^{-i\frac{2\pi}{3}} & w_0 \end{pmatrix} \delta_{\mathbf{k}+\mathbf{G}_1^M+\mathbf{G}_2^M,\mathbf{k}'} \right] a_{m,\xi,\mathbf{k}'} + h.c. \quad (\text{S70})$$

The parameters are the same as TBG. To remove the divergence at Dirac points, we add a $C_2\mathcal{T}$ breaking term $\Delta_z = 15$ meV on the bottom layer as $\Delta_z \sigma_z$. This term originates from the effect of hBN or electron-electron interaction [5].

We can calculate the orbital magnetic moment of the electrons after diagonalizing the continuum Hamiltonian. The momentum-dependent orbital moment for band n can be derived as

$$m_n(\mathbf{k}) = \frac{e}{\hbar} \sum_{m \neq n} \text{Im} \frac{\langle u_n(\mathbf{k}) | \partial_{k_x} H(\mathbf{k}) | u_m(\mathbf{k}) \rangle \langle u_m(\mathbf{k}) | \partial_{k_y} H(\mathbf{k}) | u_n(\mathbf{k}) \rangle}{\varepsilon_n(\mathbf{k}) - \varepsilon_m(\mathbf{k})}, \quad (\text{S71})$$

where $H(\mathbf{k})$ is the corresponding continuum Hamiltonian with eigenstate $|u_n(\mathbf{k})\rangle$ and eigenvalues $\varepsilon_n(\mathbf{k})$.

B. GL coefficient of superconducting twisted trilayer graphene

In this section, we provide the calculation of the Ginzburg-Landau terms $\lambda_c, \alpha, \bar{\mathcal{G}}, \bar{\mathcal{D}}$ in twisted trilayer graphene (TTG) in detail. Considering the superconductivity occurs on the conduction band, the mean-field BdG Hamiltonian of TTBG can be written as

$$H_{\text{BdG}} = \begin{pmatrix} E_{+\uparrow,\mathbf{k}} - \mu & 0 & 0 & \Delta \\ 0 & E_{-\downarrow,\mathbf{k}} - \mu & -\Delta & 0 \\ 0 & -\Delta & -E_{+\uparrow,-\mathbf{k}} + \mu & 0 \\ \Delta & 0 & 0 & -E_{-\downarrow,-\mathbf{k}} + \mu \end{pmatrix}. \quad (\text{S72})$$

Here $+(-)$ and $\uparrow(\downarrow)$ are the valley and spin index, respectively. E is the energy spectrum of the highest valence band of TTBG. Due to the time-reversal symmetry, we have $E_{+\uparrow,\mathbf{k}} = E_{-\downarrow,-\mathbf{k}}$ and $E_{-\downarrow,\mathbf{k}} = E_{+\uparrow,-\mathbf{k}}$. The mean-field

transition temperature T_c can be solved self-consistently by $1 = U \sum_{\mathbf{k}} 1/[2(E_{+\uparrow, \mathbf{k}} - \mu)] \tanh \frac{\beta_c(E_{+\uparrow, \mathbf{k}} - \mu)}{2}$, with U being the interaction strength. We choose $\mu = 1.8$ meV in the half-filling regime. In Fig. S3(a)-(c) we show the moiré bands (the lowest two flat bands), Fermi surface at half filling and the momentum-space quantum metric for the conduction band.

We summarize the calculations of $\lambda_c, \alpha, \bar{\mathcal{G}}, \bar{\mathcal{D}}$ in Fig. S3 (d)-(f). In Fig. S3 (d), $\bar{\mathcal{G}}$ is small comparing to λ_c for small U . When U increases, λ_c decays as $1/U^2$ while $\bar{\mathcal{G}}$ reaches the ideal value. This implies that the conventional term λ_c may still dominate in the experimental regime for small U . For large U , $\lambda_c \ll \bar{\mathcal{G}}$. Fig. S3 (e),(f) shows that for small U , the Fermi surface asymmetry terms α dominate over the quantum metric dipole $\bar{\mathcal{D}}$. However, When U is large, the $\bar{\mathcal{D}}$ dominate over α and $\alpha/\bar{\mathcal{D}} \sim \mathcal{O}(\beta_c^2)$. This is in agreement with the previous discussion. In the strong coupling limit, the quantum geometry effect becomes the leading order.

-
- [S1] M. V. Sadovskii, *Diagrammatics: lectures on selected problems in condensed matter theory* (World Scientific, 2006).
[S2] R. Wakatsuki, Y. Saito, S. Hoshino, Y. M. Itahashi, T. Ideue, M. Ezawa, Y. Iwasa, and N. Nagaosa, *Science advances* **3**, e1602390 (2017).
[S3] S. Yang, Z.-C. Gu, K. Sun, and S. D. Sarma, *Physical Review B* **86**, 241112 (2012).
[S4] R. Bistritzer and A. H. MacDonald, *Proceedings of the National Academy of Sciences* **108**, 12233 (2011).
[S5] M. Xie and A. H. MacDonald, *Physical review letters* **124**, 097601 (2020).